Materials Chemistry and Physics 135 (2012) 798–805

Contents lists available at SciVerse ScienceDirect

Materials Chemistry and Physics

journal homepage: www.elsevier.com/locate/matchemphys

Dielectric response, functionality and energy storage in epoxy nanocomposites: Barium titanate vs exfoliated graphite nanoplatelets

A.C. Patsidis [a,b], K. Kalaitzidou [b], G.C. Psarras [a,*]

[a] Department of Materials Science, University of Patras, Patras, Greece
[b] Woodruff School of Mechanical Engineering, Georgia Institute of Technology, Atlanta, USA

HIGHLIGHTS

- Relaxation phenomena were found to be present in all studied systems.
- Two processes emanate from the polymer matrix (α-mode and β-mode).
- Systems' electrical heterogeneity gives rise to interfacial polarization.
- $BaTiO_3$/epoxy composites exhibit functional behavior due to structural changes.
- xGnP/epoxy composites exhibit increased energy storing efficiency.

GRAPHICAL ABSTRACT

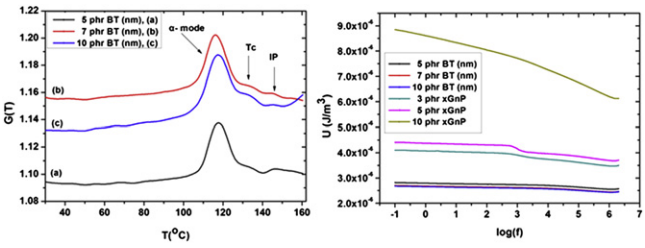

ARTICLE INFO

Article history:
Received 21 February 2012
Received in revised form
25 April 2012
Accepted 19 May 2012

Keywords:
Polymer nanocomposites
Dielectric relaxations
Ferroelectrics
Functional materials
Graphite nanoplatelets

ABSTRACT

Barium titanate/epoxy and exfoliated graphite nanoplatelets/epoxy nanocomposites were prepared and studied varying the filler content. Morphological characteristics were examined via scanning electron microscopy, while structural changes occurring in barium titanate as a function of temperature were investigated by means of X-ray diffraction. Broadband dielectric spectroscopy was employed for determining the dielectric response of the prepared systems. Based on the conducted analysis it was found that three relaxation processes are present in the spectra of the examined materials. From the slower to the faster one, these are interfacial polarization, glass to rubber transition of the polymer matrix, and rearrangement of polar side groups of the polymer chain. Systems' functionality and energy storing efficiency were assessed in terms of dielectric reinforcing function. Finally, the energy density of all systems was evaluated. Composite systems with embedded graphite nanoplatelets exhibit higher energy storing efficiency, while thermally induced structural changes in ferroelectric particles provide functional behavior to barium titanate composites.

1. Introduction

Polymer matrix nanoreinforced composites attract significant scientific and technological attention because of both the versatility of improved properties and their current or potential applications [1–10]. Nanodispersions within a polymer matrix offer the possibility to exploit the filler's pronounced surface area to volume ratio, achieving thus improved thermomechanical, rheological, electrical and optical behavior. The employed nanoinclusions can be divided with respect to their electrical nature in to two main categories: conductive, including metals and various allotropic types of carbon and non-conductive such as layered silicates, piezoelectric and ferroelectric ceramics which exhibit dielectric behavior, that is are able to be polarized under the influence of an external electric field.

Current applications of inorganic-polymer nanocomposites, include packaging, electromagnetic radiation shielding, circuit board, interlayer dielectrics, leakage current controllers, self-

* Corresponding author. Tel.: +30 2610 969347; fax: +30 2610 969372.
E-mail address: G.C.Psarras@upatras.gr (G.C. Psarras).

0254-0584/$ – see front matter © 2012 Elsevier B.V. All rights reserved.
doi:10.1016/j.matchemphys.2012.05.060

current regulators, passive protection etc [4,5,11–14]. Nowadays a lot of research is carried out in developing compact systems with integrated nanocapacitors, which could act as electrical energy storing devices [3,15–17]. The latter could be used in emerging technological applications such as cellular phones, wireless personal digital assistants, acoustic emission sensors, stationary power systems and hybrid electric vehicles [3,5,18,19].

Materials used in the above applications should exhibit high electric energy storing capability, which requires high electric field and/or high dielectric permittivity. Dielectric strength, defined as the upper limit of the applied field, above which dielectric breakdown occurs and the material stops being operational, estimates the maximum applied field. Optimum behavior is achieved by employing materials that demonstrate both high dielectric strength and permittivity. Such materials are polymer nanocomposites reinforced with ceramic polar oxides or ceramic ferroelectrics that in addition to the above they exhibit flexibility, processability, light weight, resistance to corrosion, good mechanical behavior, high dielectric breakdown strength, low cost, and high dielectric permittivity. Further, embedding ferroelectric elements within the polymer matrix adds functionality to the composite system because of the change from ferroelectric to paraelectric phase of the inclusions, at a critical temperature known as Curie temperature (T_C) [20,21]. This structural change from the low to the high symmetry lattice is a first order transition and affects the electrical performance of the system. In addition to ceramic filled polymer systems, polymer composites containing conductive fillers at concentrations around the percolation threshold are also of main technological importance because of their high dielectric permittivity values [22–24].

The focus of this study is to characterize the dielectric response, functionality and energy storing efficiency of epoxy based nanocomposites reinforced with either barium titanate ($BaTiO_3$) nanoparticles or exfoliated graphite nanoplatelets (xGnP). The effect of the filler type, concentration and size on the dielectric response and functionality of the nanocomposites was determined by means of broadband dielectric spectroscopy (BDS) in a wide frequency and temperature range by employing dielectric permittivity and electric modulus formalisms and by means of dielectric reinforcing function. The energy storing efficiency of the nanocomposites was assessed by calculating the electric energy density. The morphology of the prepared systems was examined via scanning electron microscopy (SEM) and X-ray diffraction (XRD).

2. Experimental

2.1. Materials

Nanocomposite specimens were prepared by employing commercially available materials. In particular, a low viscosity epoxy resin with the trade name Araldite LY 1564 and curing agent Aradur-HY2954 provided by Huntsman Advanced Materials were used as matrix. In addition two types of reinforcements were used, ceramic $BaTiO_3$, supplied by Sigma Aldrich, and xGnP supplied by XG Sciences (East Lansing, MI). Aiming to study the effect of the filler's size upon the dielectric properties two different powder sizes of $BaTiO_3$ were used. One with a mean particle diameter less than 2 μm and another that has mean particle diameter in the range of 30–50 nm. xGnP have mean diameter less than 1 μm and an average thickness of 10–20 nm.

2.2. Fabrication of composites

The solution method was used to fabricate the composites. Nano-filler inclusions (ceramic or carbon) were mixed for 30 min at ambient temperature with isopropyl alcohol (IPA) using a sonication probe (1/2″ probe size, 40% amplitude for 40 min, Misonix 4000) in order to breakdown the filler agglomerates. The powder was collected after filtering the IPA and mixed with the epoxy at 800 rpm and $T = 60$ °C for 1 h using a magnetic stirring plate. The curing agent was then added to the filler/monomer solution and mixing at 800 rpm and ambient temperature continued for 30 min. The mixture was degassed in a vacuum oven, casted in a mold and cured at $T = 80$ °C for 1 h followed by post curing at $T = 100$ °C for 4 h. The employed filler contents expressed in wt% of particles per hundred parts of resin (phr) are listed in Table 1.

2.3. Characterization techniques

The morphology of the composites including the presence of voids and agglomerates and the quality of the filler dispersion within the polymer matrix was assessed by SEM (Zeiss SEM Ultra 60). The crystalline structure of the ceramic powders was investigated via X-ray diffraction, using a D8 Advance (Bruker AXS) with a CuKa source (1.54 Å, 1.6 kW power), in order to detect the transition from the non-symmetrical, polar structure (ferroelectric phase) to the symmetrical, non-polar structure (paraelectric phase) of $BaTiO_3$. The electrical characterization of the composites was conducted by means of Broadband Dielectric Spectroscopy (BDS) in the frequency range of 0.1 Hz to 10 MHz, using Alpha-N Frequency Response Analyser and a 1200 BDS dielectric cell provided by Novocontrol. Isothermal frequency scans were conducted, for each specimen, from ambient temperature to 160 °C with a step of 5 °C. Novotherm system supplied also by Novocontrol was used to control the temperature.

3. Results and discussion

Representative SEM micrographs of the fracture surface of the examined systems are shown in Fig. 1. Fig. 1(a) refers to neat epoxy, while Fig. 1(b) and (c) to the 5 phr nano-$BaTiO_3$/epoxy system at low and high magnification, and Fig. 1(d) and (e) to the 5 phr xGnP/epoxy system at low and high magnification respectively. As depicted the $BaTiO_3$ powder is homogeneously distributed but as agglomerates not as single particles considering that individual particles have a diameter in the range of 30–50 nm. The same trend is observed in case of xGnP/epoxy composites. The diameter of the graphite platelets depicted in Fig. 1(c) is less than 1 μm however, their thickness is significantly larger than 10–20 nm indicating presence of agglomerates due to strong van der Waals forces among adjacent graphite platelets. It is also noted that there are voids at the xGnP/epoxy interface as a result of weak interfacial interactions.

XRD patterns of $BaTiO_3$ nano- and micro-size particles at $T = 40$ °C and $T = 170$ °C, shown in Fig. 2 reveal the structural

Table 1
Type and concentration of the reinforcing phase, for all the examined systems. Values of activation energy, for each system, as resulted by fitting data via equation (5).

Sample	E_A (eV)
Neat epoxy	0.503
5 (nm) $BaTiO_3$/epoxy	1.225
7 (nm) $BaTiO_3$/epoxy	1.225
10 (nm) $BaTiO_3$/epoxy	1.270
7 (μm) $BaTiO_3$/epoxy	1.240
10 (μm) $BaTiO_3$/epoxy	1.188
3 xGnP/epoxy	1.747
5 xGnP/epoxy	1.914
10 xGnP/epoxy	1.603

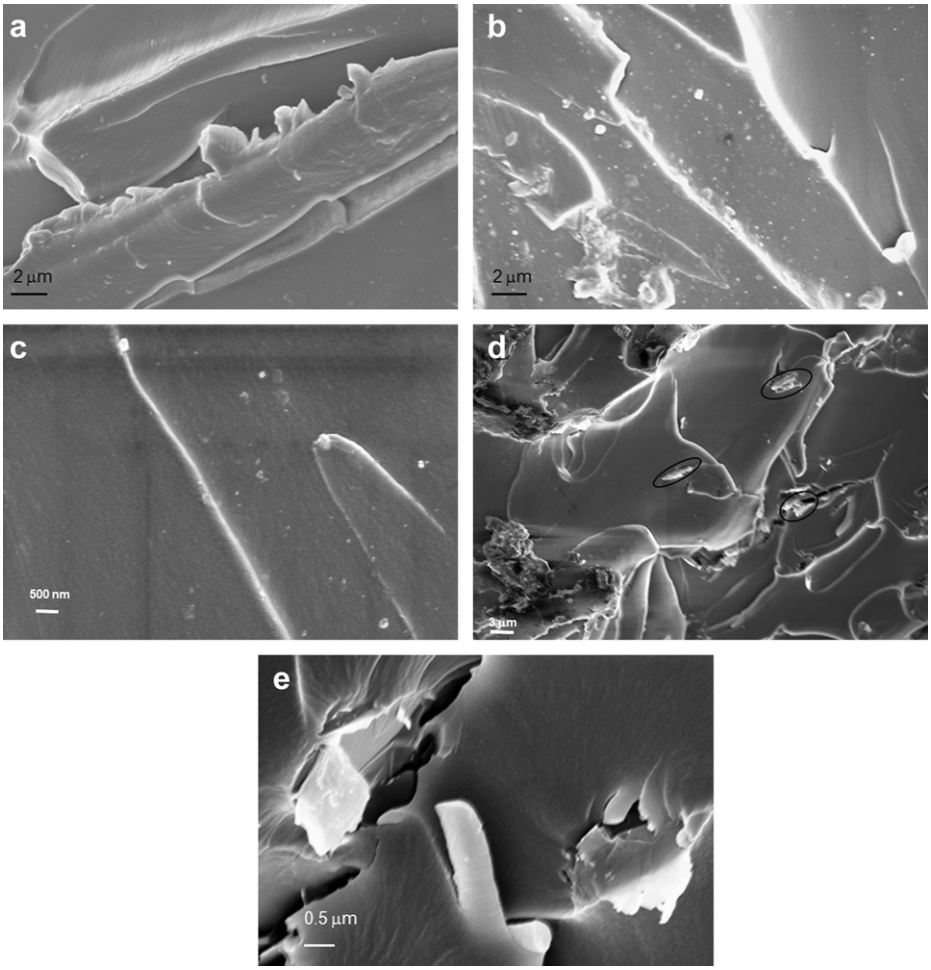

Fig. 1. SEM images of (a) pure epoxy, (b) and (c) composite with 5 phr nano-$BaTiO_3$ at low and high magnification, (d) and (e) composite with 5 phr xGnP at low and high magnification (xGnP platelets are encircled for clarity).

transition of the particles from the non-symmetrical polar tetragonal phase (ferroelectric phase) to the symmetrical non-polar cubic phase (paraelectric phase). As reported, for micro-sized $BaTiO_3$ particles this transition occurs at the critical Curie temperature ($T_C \cong 130$ °C) and although, it can be detected by the occurring changes in many physical properties in the vicinity of T_C, the best way is to examine the fingerprint of the tetragonal and cubic lattice via their XRD traces [25–31]. Far below T_C, the XRD spectrum of micro-sized $BaTiO_3$ provides the fingerprint of the fully tetragonal phase defined by the two distinct peaks at 44.9° and 45.4° [26,29,30]. On the other hand above T_C only a single narrow peak at 45.2°, which is considered as the fingerprint of the 100% cubic phase [29,30] is present. In the case of nano-sized $BaTiO_3$, the XRD spectrum at $T = 40$ °C, well below T_C deviates from the patterns of both the 100% tetragonal and 100% cubic phase. The nano-$BaTiO_3$ trace forms a broad and non-symmetrical peak, which can be considered as double, in the range between the two peaks of the tetragonal phase. The absence of clear "tetragonal" or "cubic" trace indicates the co-existence of both phases. Further, above T_C the nano-spectrum approaches significantly the cubic pattern, implying that part of the nano-sized $BaTiO_3$ particles underwent the ferroelectric to paraelectric transition. It should be noted that the length scale of the ferroelectric particles is related with the type of their lattice. Below T_C nano-sized $BaTiO_3$ forms cubic crystals. The existence or not of a critical size beyond which tetragonal phase is no longer present is still an open question [27,28,30,32]. Lack of non-symmetrical to symmetrical structural change diminishes the functionality of the ceramic particles, and consequently the functionality of the composite systems.

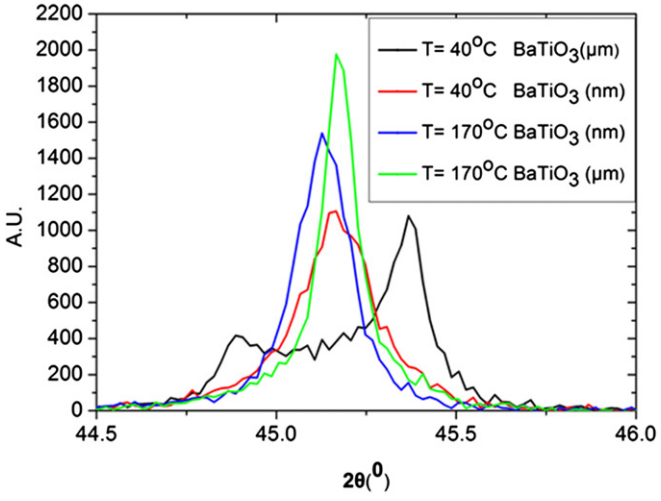

Fig. 2. XRD spectra of the micro- and nano-$BaTiO_3$ particles at 40 °C and 170 °C.

Dielectric relaxations present in the dielectric spectra of polymer composites arise from the polymer matrix, interfacial

phenomena and conductivity effects. In this study dielectric data was first expressed in terms of the real and imaginary part of dielectric permittivity and transformed in the electric modulus presentation. Electric modulus is defined as the inverse quantity of the complex dielectric permittivity. Electric modulus formalism has been proved suitable for describing dielectric relaxation processes, especially in the low frequency range and at high temperatures, where both real and imaginary part of dielectric permittivity attain often high values. The main contribution of electric modulus is that it neglects the influence of electrode polarization upon dielectric data. Arguments for the resulting benefits have been exhibited and discussed elsewhere [33–36].

Fig. 3 depicts the variation of the real part of dielectric permittivity with frequency at two different temperatures, for all the types of the examined systems. The influence of reinforcing phase becomes evident via the enhancement of (ε') with filler content. Real part of dielectric permittivity increases with frequency diminishing and with rise of temperature. This is expected, since epsilon prime reflects the level of the achieved polarization. When frequency is low, permanent and induced dipoles acquire sufficient time to align themselves parallel to the applied field; further higher temperatures offer thermal agitation which facilitates the orientation of the dipoles. Fig. 3(a) and (b) denotes that the effect of xGnP inclusions is more pronounced with respect to the effect of nano- or micro-size $BaTiO_3$ particles. Conductivity of xGnP is much higher than the corresponding of $BaTiO_3$, since the latter is a wide band gap semiconductor. Thus, xGnP/polymer nanosystems are characterized by enhanced electrical heterogeneity and interfacial polarization should play a crucial role in their electrical response.

Interfacial polarization (IP), also known as Maxwell–Wagner–Sillars effect, appears in heterogeneous systems via the accumulation of unbounded charges at the interfaces of the systems' constituents, where they form large dipoles. The latter are rather large compared to other types of dipoles and thus are characterized by increased inertia in responding to the applied field. IP is a slow relaxation process, occurring in the low frequency range and at high temperatures, resulting in enhanced permittivity values. Polymer systems and composites exhibit IP because of the presence of additives, plasticizers and fillers. Further to IP, embedding conductive inclusions into an insulating polymer matrix increases the overall conductivity of the composite systems, resulting again to higher values of permittivity [33,37]. In the case of the xGnP/epoxy composites there is a systematic increase of (ε') with filler content.

However, in the case of $BaTiO_3$/epoxy composites, this is confirmed only for filler concentrations up to 7 phr. At higher concentrations for both nano- and micro-particles, (ε') diminishes with filler content. Concerning a binary system of two components varying significantly in permittivity values, one should expect that the permittivity of the whole system should increase monotonically with the concentration of the high permittivity constituent [14,33,37]. Since dielectric permittivity of $BaTiO_3$ is much higher than that of epoxy resin the recorded behavior for the filler concentration up to 7 phr, in Fig. 3(c) is quite understandable. However, such an approach ignores the influence of particles distribution and interfacial interactions between matrix and filler. Examples of reduced permittivity with filler content in polar oxides/epoxy composites have been reported in the literature [1,3,38].

Lowering of (ε') corresponds to reduction of polarization, which can be caused by an orientation obstruction of polar groups, and/or presence of voids, extensive agglomerates via insufficient distribution and poor matrix-filler adhesion. In our case specimens with 10 phr of either micro- or nano-$BaTiO_3$ particles demonstrate a decrease to dielectric permittivity values, indicating indirectly that the optimum reinforcing concentration, for the specific

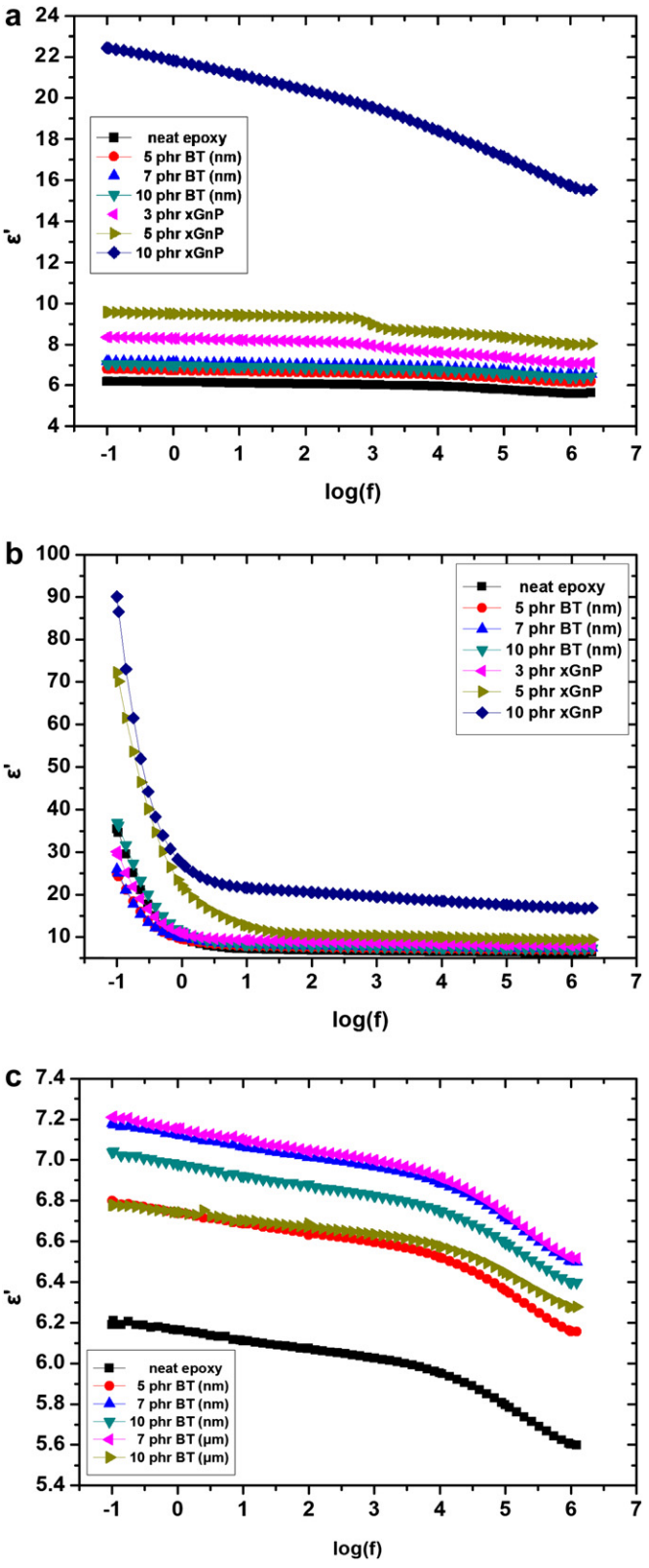

Fig. 3. Variation of the real part of dielectric permittivity for the $BaTiO_3$/epoxy and xGnP/epoxy nanocomposites (a) at 30 °C, (b) at 150 °C, and (c) for the $BaTiO_3$/epoxy systems at 30 °C.

composite system, is lower than 10 phr. The effect of $BaTiO_3$ size on the real part of the dielectric permittivity can be seen in Fig. 3(a). For the same filler content and at the same temperature it becomes evident that micro-composites exhibit higher permittivity than nanocomposites, denoting a higher level of polarization. The latter most probably is related to the higher polar nature (pure tetragonal lattice) of the micro-particles.

Typical plots of the recorded dielectric relaxation phenomena in the examined set of composite systems are given in Figs. 4–6. Fig. 4(a) and (b) depicts the variation of real and imaginary part of electric modulus, for the pure resin specimen as a function of frequency at different temperatures. While Figs. 5 and 6 show the same variation for the 7 phr (nano) $BaTiO_3$/epoxy and the 10 phr xGnP/epoxy systems, respectively. Relaxation processes can be detected from the step-like transition from low to high values of (M') and the formation of peaks, in the temperature range of the transition, in the electric modulus loss index (M'') plots. In all three examples at least two processes can be detected. The major one appears at temperatures higher than 110 °C in the low frequency range, while a much weaker process can be observed at the high frequency regime and at temperatures lower than 90 °C. Since both modes are present in the pure epoxy resin spectra, they are due to processes occurring in the polymer matrix. The weak and relative fast one, occurring at high frequencies, could be attributed to the

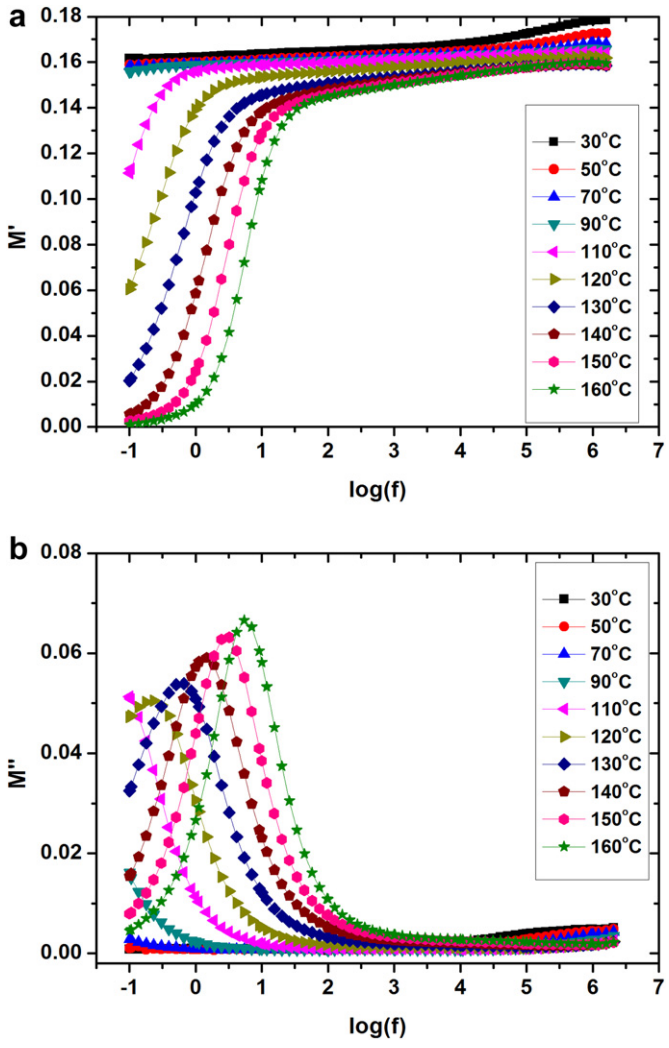

Fig. 4. Real (a) and imaginary (b) part of electric modulus vs frequency, at various temperatures for the neat epoxy resin.

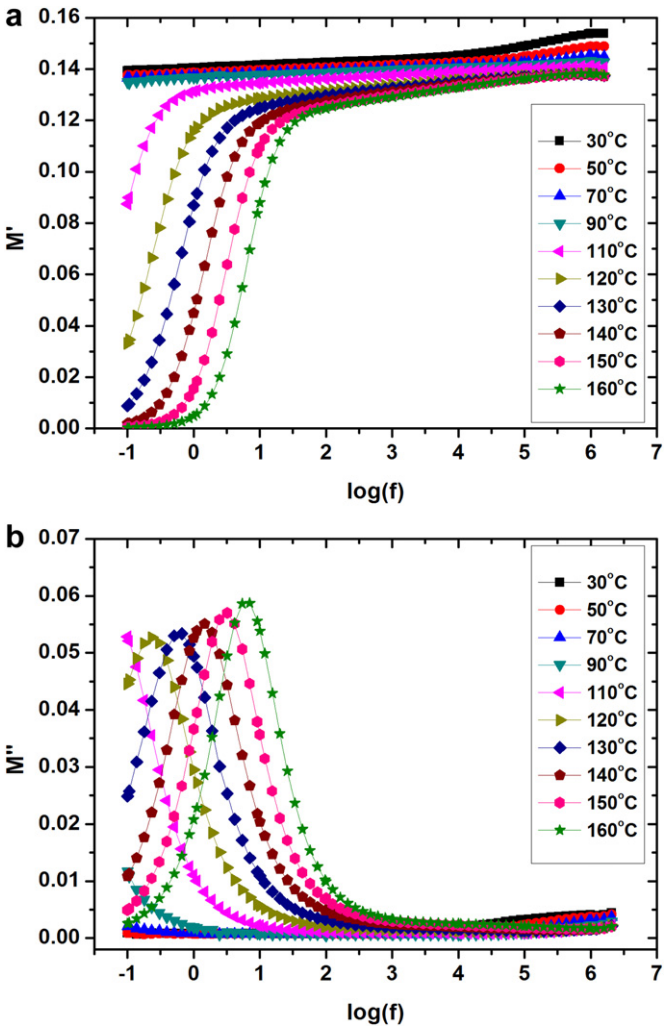

Fig. 5. Real (a) and imaginary (b) part of electric modulus vs frequency, at various temperatures for the 7 phr nano-$BaTiO_3$/epoxy system.

rearrangement of polar side groups of the main polymer chains (β-mode). On the other hand, the slow and intensive process, recorded at low frequencies, should be connected with the glass to rubber transition of the polymer matrix (α-mode). In composite systems, and especially in the systems with enhanced electrical heterogeneity, IP is expected to be present. Glass to rubber transition temperature of the employed epoxy resin has been found close to 125 °C [39]. Thus, IP and glass to rubber transition are both slow processes occurring in the same frequency and temperature range, being possibly superimposed.

Functional behavior of composites can be ascribed to the variation of different physical properties, such as polarization or conductivity, with frequency and temperature. In the present study the amplitude of the applied voltage was kept constant and low (1000 mV). However, small variations in the samples' thickness modified the exerted field from specimen to specimen. Fig. 7 presents the dielectric response of the examined systems in terms of the Dielectric Reinforcing Function (DRF). DRF introduced recently [40] aims to remove the influence of geometrical characteristics upon the produced polarization and connects functional behavior with materials properties. DRF is defined [40] as follows:

$$G(\omega, T) = \frac{\varepsilon'_{comp}(\omega, T)}{\varepsilon'_{mat}(\omega, T)} \quad (1)$$

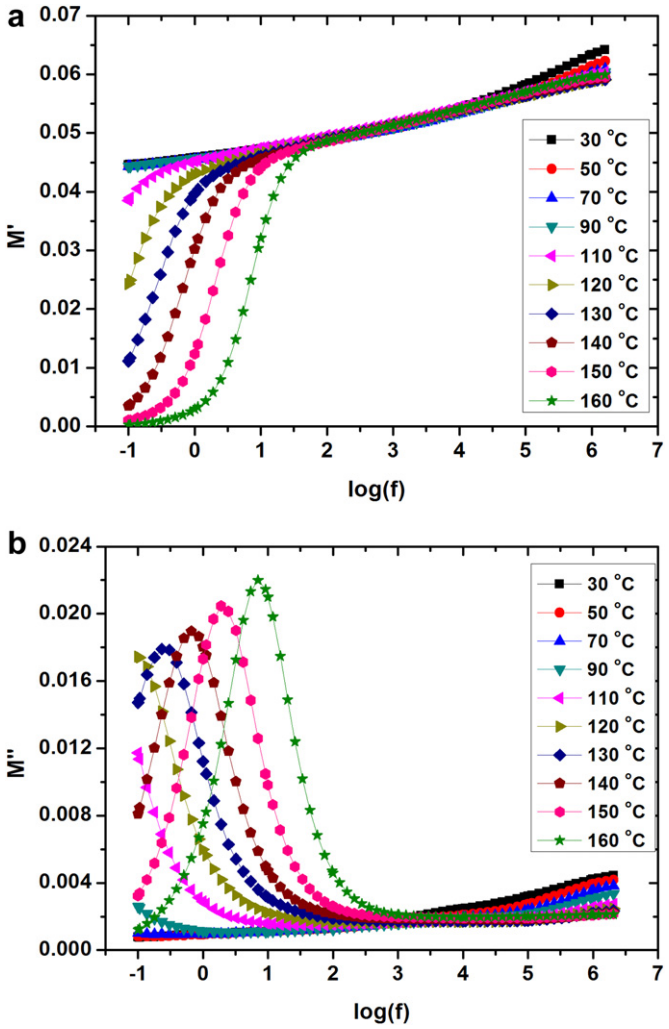

Fig. 6. Real (a) and imaginary (b) part of electric modulus vs frequency, at various temperatures for the 10 phr xGnP/epoxy system.

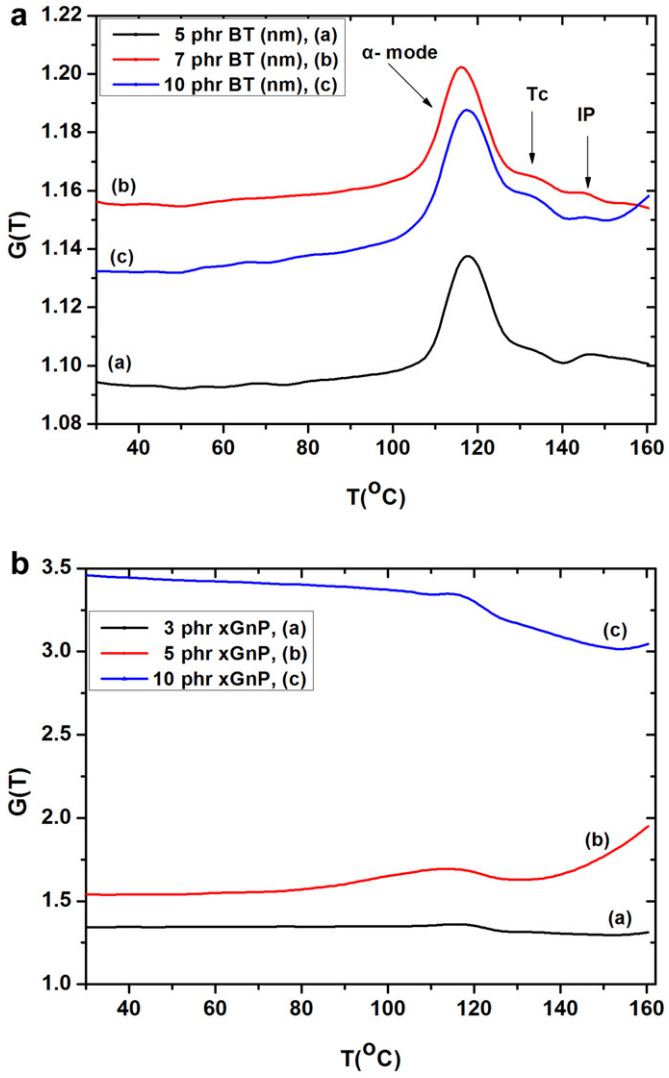

Fig. 7. DRF vs temperature for the (a) $BaTiO_3$/epoxy and (b) xGnP/epoxy nanocomposites at 10 Hz.

where $\varepsilon'_{comp}(\omega, T)$ and $\varepsilon'_{mat}(\omega, T)$ are the real part of the dielectric permittivity of the composite and the matrix respectively, while ω is the angular frequency of the field and T the sample's temperature. Under isothermal or isochronal conditions the previous expression takes the following forms:

$$G(\omega)|_T = \frac{\varepsilon'_{comp}(\omega)}{\varepsilon'_{mat}(\omega)} \quad (2)$$

$$G(T)|_\omega = \frac{\varepsilon'_{comp}(T)}{\varepsilon'_{mat}(T)} \quad (3)$$

DRF is a measure of the normalized polarization, reflecting the dielectric strengthening of the reinforcing phase, and the level of the energy storing efficiency [40]. Fig. 7(a) and (b) presents the variation of DRF with temperature at constant frequency $f = 10$ Hz for the $BaTiO_3$ and xGnP reinforced nanocomposites respectively. Systems containing xGnP attain much higher values than systems with $BaTiO_3$, and specifically, in the case of the maximum xGnP loading the $G(T)$ values are three times higher than those of the $BaTiO_3$ system. This difference implies the difference in the energy storing efficiency of the systems. As already mentioned the enhanced conductivity of the graphite nanoplatelets can be considered as the origin of this behavior. DRF spectra of the $BaTiO_3$/epoxy systems, besides their lower values, exhibit peaks and "humps", which correspond to processes related to variations of polarization. In the low frequency range and at temperatures higher than 100 °C, three dynamic polarization mechanisms are present. Glass to rubber transition is the first one and is recorded in the vicinity of the glass transition temperature of the polymer matrix (T_g). Since T_g of the employed polymer matrix found to be close to 125 °C [39], the formed peaks in Fig. 7(a), which lie very close to 120 °C, are attributed to α-relaxation process. The second mechanism is IP, which is an even slower process occurring at high temperatures and low frequencies. Finally, the third dynamic polarization mechanism reflects the transition from ferroelectric to paraelectric phase at T_C. The simultaneous occurrence of all three mechanisms makes their discrimination not easy. However, their dynamics should vary at different rates, and thus at a suitable temperature-frequency "snapshot" a rough distinction can be recorded. Consequently the "hump" next to the peak, in the spectra of $G(T)$ in Fig. 7(a), is ascribed to ferroelectric to paraelectric transition of $BaTiO_3$, while the less intensive peak at higher

temperatures to IP. On the other hand, the xGnP/epoxy spectra, Fig. 7(b), attain rather constant values almost up to the T_g of the matrix, where it plateaus. At temperatures close to T_g or higher, the mobility of large parts of the polymer chains increases significantly, affecting the achieved polarization, while IP contributes also to the tendency to achieve higher values of polarization.

The electric energy density of a dielectric material is given by equation (4) [16,41]:

$$U = \frac{1}{2}\varepsilon_0 \varepsilon' E^2 \tag{4}$$

where ε_0 is the permittivity of vacuum and E the field's intensity. Employing equation (4) and experimental data the function of energy density for all the examined systems can be determined. It should be noted that energy density alters with both dielectric permittivity and applied field. However, the effect of field's intensity is more rapid, since it appears in equation (4) in the second order. Maximum energy density is achieved at the material's breakdown strength. In this study the applied field was low, focusing upon the influence of the materials properties on the energy storing efficiency. Materials properties are expressed in equation (4) via the real part of dielectric permittivity. Isothermal plots of the function of energy density are depicted in Fig. 8, at two different temperatures. As expected, the energy density of the xGnP/epoxy systems is much higher than that of the $BaTiO_3$/epoxy systems in the whole frequency range. Further, energy density increases steadily with xGnP content.

Fig. 9 shows the temperature dependence of the loss maxima for the main peak present in Figs. 4(b), 5(b) and 6(b). Fig. 9(a) depicts data and linear fitting for the pure epoxy and $BaTiO_3$/epoxy systems, while Fig. 9(b) depicts the same for the xGnP/epoxy systems. In all cases, data can be described by equation (5), implying an Arrhenius type behavior

$$f_{max} = f_0 \exp\left(-\frac{E_A}{k_B T}\right) \tag{5}$$

where E_A is the activation energy, f_0 a pre-exponential factor, and k_B the Boltzmann constant. Values of activation energy calculated via the regression of equation (5) are listed in Table 1. It is apparent that the response of the polymer matrix deviates significantly from the response of all the composite systems. From the conducted analysis the main loss peak recorded at low frequencies and high temperatures has been attributed to superposition of α-process and IP. It is

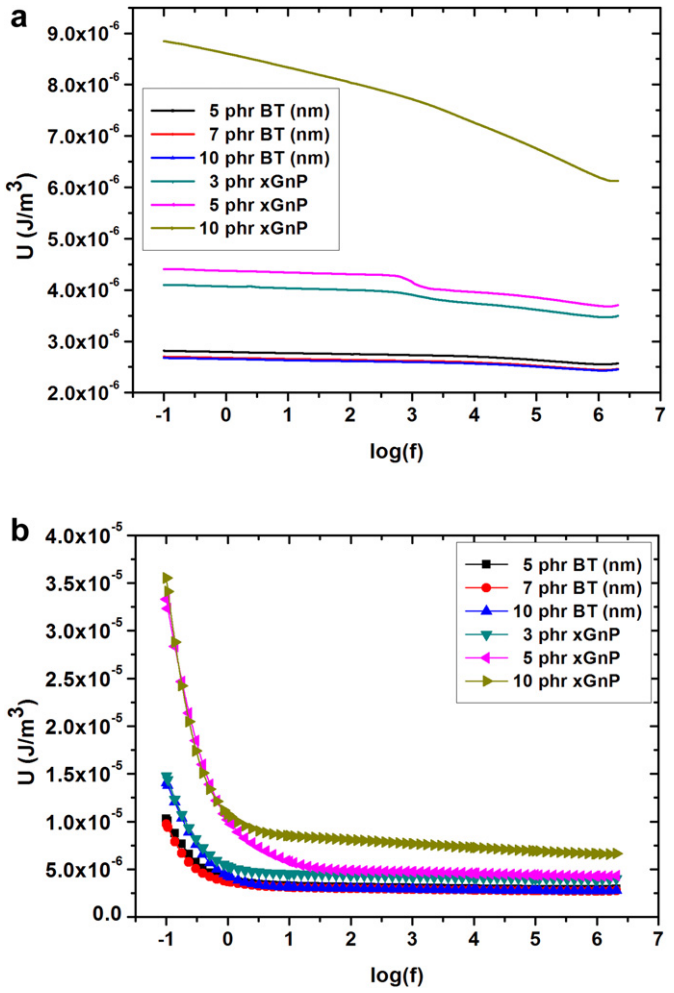

Fig. 8. Energy density vs frequency, for all the examined nanocomposites, at (a) 30 °C, and (b) 150 °C.

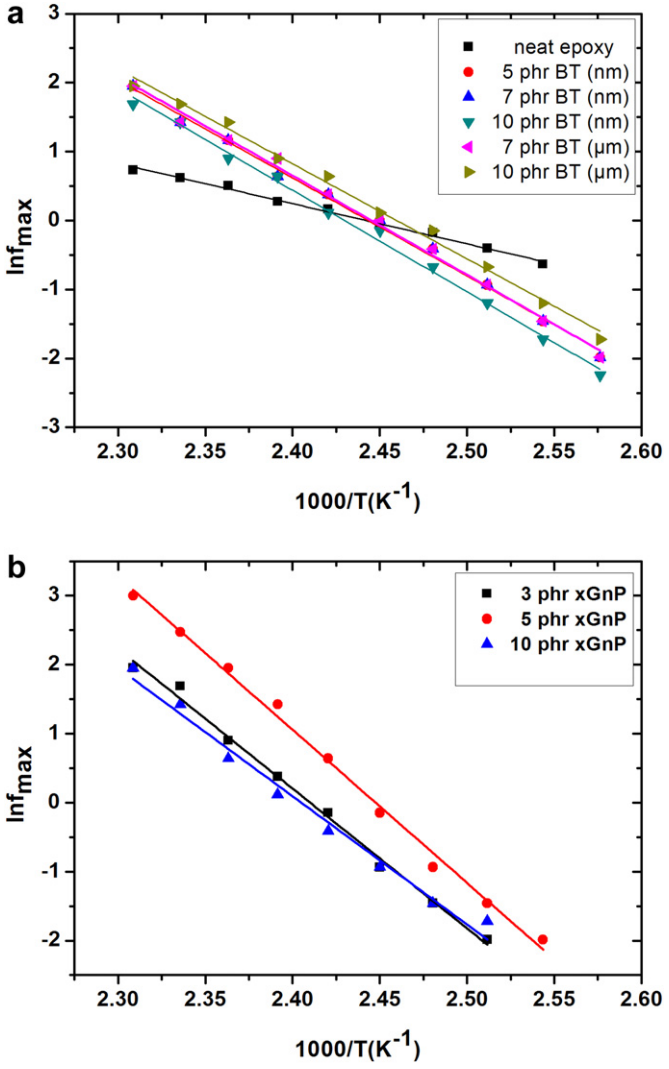

Fig. 9. Loss peak position as a function of the inverse temperature for (a) neat epoxy and $BaTiO_3$/epoxy composites, and (b) xGnP/epoxy composites, for the main loss peak.

well accepted [14,34,35] that the loss peak dependence on reciprocal temperature for α-relaxation process deviates from an Arrhenius type behavior, while IP exhibits Arrhenius response. The linear dependence in Fig. 9(a) and (b) supports indirectly that the corresponding relaxation process is related to IP. In the case of the matrix IP is much weaker, characterized by the lower activation energy, and thus is probably dominated by α-mode. In composite systems activation energy attains higher values, implying that IP is more pronounced. Activation energy is higher in the xGnP/epoxy systems following the increase of electrical heterogeneity. Composites with $BaTiO_3$ have practically constant activation energy.

4. Conclusions

$BaTiO_3$/epoxy and xGnP/epoxy nanocomposites were prepared and studied. $BaTiO_3$ particles exhibit functional behavior due to their structural transition from the ferroelectric (polar) to the paraelectric (non-polar) phase, at a critical temperature. In the dielectric spectra of all the examined systems relaxation phenomena were found to be present. Two relaxation processes emanate from the polymer matrix, which are glass to rubber transition (α-mode) and rearrangement of polar side groups (β-mode). Interfacial polarization resulting from the electrical heterogeneity of the systems occurs in the same temperature and frequency range with the α-mode, and thus their individual distinction is difficult. Dielectric reinforcing function offers the possibility to investigate the functional behavior and the energy storing efficiency of the examined systems. Composites with embedded $BaTiO_3$ particles exhibit functional versatility because of the thermally activated structural changes, which can be resembled to a molecular engine. In contrary composites with embedded xGnP exhibit increased energy storing efficiency, this appears to be constant up to T_g of the matrix. Finally, relaxation dynamics of the main loss peak appears to be connected to both α-mode and IP.

Acknowledgments

This work was enabled by financial support from the Georgia Institute of Technology Woodruff School of Mechanical Engineering and European Union and the Ministry of National Education Life Long Learning and Religious Affairs of Greece within the “THALES” research framework.

References

[1] S. Singha, M.J. Thomas, IEEE Trans. Dielectr. Electr. Insul. 15 (2008) 12–23.
[2] F.F. Fang, H.J. Choi, J. Joo, J. Nanosci. Nanotechnol. 8 (2008) 1559–1581.
[3] V. Tomer, G. Polizos, E. Manias, C.A. Randall, J. Appl. Phys. 108 (2010) 074116.
[4] M.T. Sebastian, H. Jantunen, Int. J. Appl. Ceram. Technol. 7 (2010) 415–434.
[5] L. Ramajo, M.M. Reboredo, M.S. Castro, Int. J. Appl. Ceram. Technol. 7 (2010) 444–451.
[6] G. Kortaberria, P. Arruti, I. Mondragon, L. Vescovo, M. Sangermano, J. Appl. Polym. Sci. 120 (2011) 2361–2367.
[7] L.S. Schadler, L.C. Brinson, W.G. Sawyer, J. Min. Metall. Sect. B Metall. 59 (2007) 53–60.
[8] T. Hanemann, B. Schumacher, J. Haußelt, Microelectron. Eng. 87 (2010) 15–19.
[9] T. Hanemann, H. Gesswein, B. Schumacher, Microsyst. Technol. 17 (2011) 1529–1535.
[10] W.R. Caseri, Mater. Sci. Technol. 22 (2006) 807–817.
[11] M.-A. Kakimoto, A. Takahashi, T.-A. Tsurumi, J. Hao, L. Li, R. Kikuchi, T. Miwa, T. Oono, S. Yamada, Mater. Sci. Eng. B Adv. Funct. Solid State Mater. 132 (2006) 74–78.
[12] Z.-M. Dang, Y.-F. Yu, H.-P. Xu, J. Bai, Compos. Sci. Technol. 68 (2008) 171–177.
[13] A.K. Batra, M.D. Aggarwal, M.E. Edwards, A. Bhalla, Ferroelectrics 366 (2008) 84–121.
[14] C.G. Raptis, A. Patsidis, G.C. Psarras, Express Polym. Lett. 4 (2010) 234–243.
[15] G. Polizos, V. Toner, E. Manias, C.A. Randall, J. Appl. Phys. 108 (2010) 074117.
[16] Q. Wang, L. Zhu, Polym. Phys. 49 (2011) 1421–1429.
[17] I. Asimakopoulos, L. Zoumpoulakis, G.C. Psarras, J. Appl. Polym. Sci. 125 (2012) 3737–3744.
[18] N. Korotkov, S.A. Gridnev, S.A. Konstantinov, T.I. Klimentova, Y.V. Barmin, I.V. Babkina, Ferroelectrics 299 (2004) 171–177.
[19] L. Ramajo, M. Reboredo, M. Castro, Compos. A Appl. Sci. Manuf. 36 (2005) 1267–1274.
[20] J.I. Gersten, F.W. Smith, The Physics and Chemistry of Materials, Wiley, New York, 2001.
[21] A. Patsidis, G.C. Psarras, Express Polym. Lett. 2 (2008) 718–726.
[22] V. Panwar, R.M. Mehra, Eur. Polym. J. 44 (2008) 2367–2375.
[23] F. He, S. Lau, H. Laiwa Chan, J. Fan, Adv. Mater. 21 (2009) 710–715.
[24] S.C. Tjong, in: S.C. Tjong, Y.-W. Mai (Eds.), Physical Properties and Applications of Polymer Nanocomposites, Woodhead Publishing Co., Oxford, 2010, pp. 495–539.
[25] B.D. Begg, E.R. Vance, J. Nowotny, J. Am. Ceram. Soc. 77 (1994) 3186–3192.
[26] P.K. Dutta, R. Asiaie, S.A. Akbar, W. Zhu, Chem. Mater. 6 (1994) 1542–1548.
[27] M.B. Smith, K. Page, T. Siegrist, P.L. Redmond, E.C. Walter, R. Seshadri, L.E. Brus, M.L. Steigerwald, J. Am. Ceram. Soc. 130 (2008) 6955–6963.
[28] H.R. Xu, L. Gao, J. Am. Ceram. Soc. 86 (2003) 203–205.
[29] F. Baeten, B. Derks, W. Coppens, E. van Kleef, J. Eur. Ceram. Soc. 26 (2006) 589–592.
[30] T.K. Mandal, Mater. Lett. 61 (2007) 850–854.
[31] A.C. Patsidis, G.C. Psarras, 5th International Conference on Emerging Technologies in Non-destructive Testing, ETNCT5, September 19–21 2011, Ioannina, Greece.
[32] B. Shumacher, H. Gebwein, J. Haubelt, T. Hanemann, Microelectron. Eng. 87 (2010) 1978–1983.
[33] G.M. Tsangaris, G.C. Psarras, N. Kouloumbi, J. Mater. Sci. 33 (1998) 2027–2037.
[34] G.A. Kontos, A.L. Soulintzis, P.K. Karahaliou, G.C. Psarras, S.N. Georga, C.A. Krontiras, M.N. Pisanias, Express Polym. Lett. 1 (2007) 781–789.
[35] M. Hernandez, J. Carretero-Gonzalez, R. Verdejo, T.A. Ezquerra, M.L.A. Lopez-Manchado, Macromolecules 43 (2010) 643–651.
[36] J. Belattar, M.E. Achour, C. Brosseau, J. Appl. Phys. 110 (2011) 054101.
[37] G.M. Tsangaris, G.C. Psarras, N. Kouloumbi, Mater. Sci. Technol. 12 (1996) 533–538.
[38] S. Singha, M.J. Thomas, A. Kulkarni, IEEE Trans. Dielectr. Electr. Insul. 17 (2010) 1249–1258.
[39] A.C. Patsidis, G.C. Psarras, K. Kalaitzidou, 18th International Conference on Composite Materials, ICCM18, 21–26 August 2011, (Jeju, Korea).
[40] G. Ioannou, A. Patsidis, G.C. Psarras, Compos. A Appl. Sci. Manuf. 42 (2011) 104–110.
[41] Z.-M. Dang, J.-K. Yuan, J.-W. Zha, T. Zhou, S.-T. Li, G.-H. Hu, Prog. Mater. Sci. 57 (2012) 660–723.